JETIR.ORG ISSN: 2349-5162 | ESTD Year : 2014 | Monthly Issue
JOURNAL OF EMERGING TECHNOLOGIES AND INNOVATIVE RESEARCH (JETIR)
An International Scholarly Open Access, Peer-reviewed, Refereed Journal

ADAPTIVE MULTIRATE DATA ACQUISITION OF 3D CELL IMAGES

[1] Ashish G. Kokate, [2] Vinit P. Kharkar
[1,2]Assistant Professor,
[1,2]Department of Electronics and Telecommunication Engineering,
[1,2]Prof Ram Meghe College Engineering & Management, Badnera-Amravati, (M.S.), India

Abstract: We propose an algorithm for adaptive efficient acquisition of fluorescence microscopy data sets using a multirate (MR) approach. We simulate acquisition as part of a larger system for protein classification based on their subcellular location patterns and, thus, strive to maintain the achieved level of classification accuracy as much as possible. This problem is similar to image compression but unique due to additional restrictions, namely causality; we have access only to the information scanned up to that point. While we do want to acquire fewer samples with as low distortion as possible to achieve compression, our goal is to do so while affecting the overall classification accuracy as little as possible. We achieve this by using an adaptive MR scanning scheme which samples the regions of the image area that hold the most pertinent information. Our results show that we can achieve significant compression which we can then use to acquire faster or to increase space resolution of our data set, all while minimally affecting the classification accuracy of the entire system.

Index Terms **- Photobleaching, Sampling**

I. INTRODUCTION

The motivation for finding an efficient way of acquiring cellular data sets is great. In fluorescence microscopy, the confocal laser scanning microscope is one of the most often used and it scans the field line-by-line, pixel-by-pixel. Photo bleaching occurs each time the laser used to excite the region being imaged focuses on a pixel. The exposure time and laser intensity both play a major part in photo bleaching. By reducing the number of samples we need to scan, we avoid the unnecessary exposure of the specimen to light, as well as save time and, thus, speed up the acquisition process. One could reduce the number of samples acquired by using traditional sampling algorithms but effects of aliasing would distort the approximation data sets. We aim here for an adaptive, efficient algorithm that would scan fewer pixel locations, while limiting the distortion and maintaining as much information as possible about the distribution of fluorescence in the sample. This requires some means of evaluation, and for this we build on prior work demonstrating that machine classifiers can recognize all major subcellular patterns in three-dimensional (3-D) data sets of cultured cells with high accuracy as shown by Murphy and his group. We can, thus, compare the classification accuracy for adaptively sampled data sets to that for the original data sets to assess the degree of preservation of image information content. The bulk of previous work in this area focused on the process of recovery rather than data acquisition. There exist some examples of undersampling of cellular fields by simple approaches such as scanning every other line or every fourth line in a line-by-line scanning pattern. This approach could be described as efficient but most certainly not adaptive as it does not change with the input of the field. Trying to efficiently acquire cellular data sets using adaptive sampling methods is new.

We will work both with two-dimensional (2-D) data sets (slices of cell volumes) and 3-D data sets (cell volumes) of maximum resolution in each of the three dimensions and will run our multirate (MR) data acquisition algorithm using different input parameters on each of these data sets to simulate the real acquisition process. MR in this paper refers to processing at different sampling rates specific to the content present in those regions. We will then compare our adaptively sampled data sets to the original data sets and examine their rate-distortion curves to find where the algorithm works optimally. We will do the same with standard downsampling (regular sampling in each dimension) using bilinear interpolation. Although this rate-distortion measure will give a general insight into the performance of the algorithm, our goal is to eventually reduce the number of samples while minimally affecting the classification accuracy of the system. We will, thus, measure the compression ratio with respect to the classification accuracy. Eventually, our algorithm should serve as a model for guiding the microscope's scanning protocol.

I. LITERATURE SURVEY

There are a number of bio image databases available for various model organisms, including for example: the Allen Brain Atlas database (www.brain-map.org) with genome-wide in situ gene expression patterns for the mouse brain; the interactive and multiresolution database for scanned and annotated images of serial sections of both primate and non-primate brains (Brainmaps.org); the BDGP database (www.fruitfly.org) containing in situ embryogenesis gene expression patterns of about 5000 fruit fly genes; the GFP expression pattern database for C.elegans (gfpworm.org) and the ZFin FishNet (www.fishnet.org.au, Bryson- Richardson, 2007) that is a 3D database of zebrafish development from the early embryo to adult.

There is an increasing interest for research meetings in this new area. The 2005 Bioimage Informatics meeting was held at Stanford University (bioimageinformatics.org). The 2008 meeting at UC Santa Barbara attracted about 150 frontier researchers in

this field. The upcoming conference in 2009 will be held at Janelia Farm Research Campus, Howard Hughes Medical Institute. Many other events include workshops on Microscopic Image Analysis with Applications in Biology (miaab.org), several workshops related to bioimage analysis in the annual IEEE ISBI conferences (biomedicalimaging.org), NIST workshop on 2D/3D image content representation, analysis and retrieval (www.nist.gov), etc. There are several special issues of journals and books on the topics of bioimage informatics, molecular and cellular image analysis, etc. BMC Cell Biology published a special issue in 2007 (http://www.biomedcentral.com/1471-2121/8?issue=S1), including nine papers covering new image analysis and mining algorithms, data visualization, biological applications, enabling supercomputing techniques, and computer vision and machine learning methods to solve other biology problems. It also includes a short summary of the bioimage informatics challenges (Auer et al., 2007), including the demand for bioimage informatics techniques, the need of multiscale imaging, collaboration and communication between biologists and engineers, common bioimage informatics problems and bench test datasets and modeling. Other special editions include for example the IEEE Transactions on Image Processing 2005 special issue on Molecular and Cellular Bioimaging (edited by Murphy, R, Meijering, E. and Danuser, G.), etc. Artech Publishing House is going to publish a book on the Microscopic Image Analysis for Life Science Applications in 2008..

III. METHODOLOGY

3.1 Molecular Imaging

For each pixel in the cellular field, a length of time is required to excite the fluorophores present in order to emit light. The exposure time is dependent on the intensity of the laser. As illustrated in Fig. 1, the laser passes through an objective and is concentrated in the focal plane. Although the energy of the laser converges in the focal plane, the laser must still pass through the planes neighboring the focus plane. This exposure to the laser causes photobleaching effects in the neighboring planes. By acquiring fewer samples, we could reduce the intensity of the laser, thereby reducing the effects of photobleaching. The reduced number of samples could also be used to speed up the acquisition of cellular data sets when implemented on a confocal scanning microscope. Fig. 2 gives a representative image from our data sets. Observe how the image is predominantly dark with mostly low pixel intensities. We, thus, assume the following:

High frequencies (rapid changes in pixel intensities among neighboring pixels) will only occur in a small percentage of the area contained within the image boundaries. Observe also how the neighboring slices share similar shape patterns and locations in the 3-D image of actin given in Fig. 3.

With these observations in mind, we can make a strong argument for a MR approach. When standard downsampling is used and the data set is then interpolated back to the maximum resolution using bilinear interpolation, all of the high-frequency

content is lost. In the dark regions of the data sets, only low frequencies are present, which can be captured with only a few samples. In contrast, in the areas where high-intensity values are located, high frequencies reside that need to be represented using a greater number of samples. Thus, using different sampling rates in different areas of the image is warranted. We call this MR sampling.

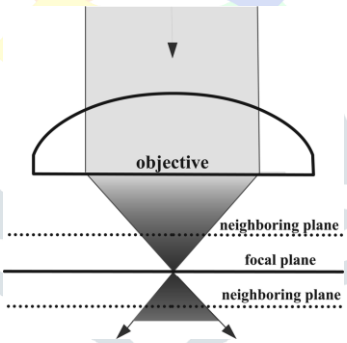

Fig. 1. Laser concentrated on the focal plane. Laser intensity increases near the focal plane.

3.2 Algorithm for MR Acquisition of Cellular Data Sets

An intuitive way to describe the algorithm is to consider the board game Battleship. The player's goal is to locate the exact locations of his/her opponent's ships in the most efficient manner possible. We draw a parallel between the game board grid and the unknown cellular field. Each consists of discrete locations and the pertinent information location is not known upon beginning the search. It would be foolish to play the game in a nonadoptive approach that is, knowing all of the locations where you will probe a priori. For example, if a ship has been hit, one would not continue with predetermined probe locations; rather, one would keep on probing in the area around the hit. Similarly, when acquiring our data sets, we keep on probing around those locations deemed significant.

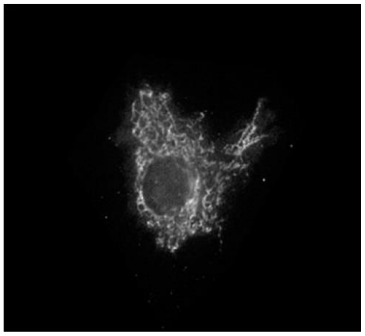

Fig. 2. Image of a mitochondrial protein pattern.

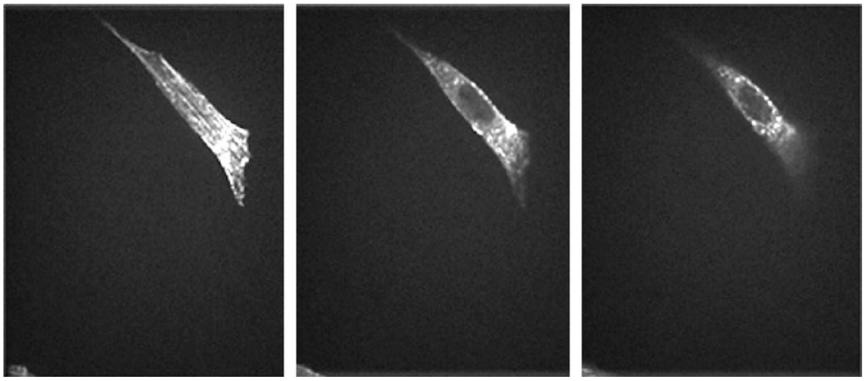

Fig. 3. Images from a 3-D sequence of actin protein pattern

We denote our 3-D data set as $x \in \mathbb{R}^{M \times N \times O}$ where $M = 2^l M_1, N = 2^l N_1$ and O denote the image size in the three spatial dimensions. The block diagram of our adaptive MR algorithm is shown in Fig. 4, and repeated for each slice of the 3-D image. This is the major component of the overall system that constructs an approximation to the original cellular data set. We now explain the algorithm in more detail. In our simulations, a probe is represented by taking a sample from the maximum resolution original image at a specific pixel location. Probe locations are initialized in one of two ways: The first is to set up probe locations throughout the entire cellular field rectangular at primary units apart (primary unit refers to the basic element of the maximum resolution), as in Fig. 5. For our experiments, we set $l = 3$ or 4 These probe locations belong to the following index set I :

$$I = \left\{ (m,n) \,\middle|\, \begin{array}{ll} m = 2^{l-1}(2k_m + 1), & k_m = 0, \ldots, M_1 - 1 \\ n = 2^{l-1}(2k_n + 1), & k_n = 0, \ldots, N_1 - 1. \end{array} \right.$$

This index set corresponds to the probing image, $p \in \mathbb{R}^{M \times N}$. Method (a) is described as

$$p^{(a)}_{m,n,o} = \begin{cases} 1, & (m,n) \in I \\ 0, & \text{otherwise.} \end{cases}$$

Thus, $p^{(a)}_{m,n,o}$ would be equal to 1 in black box locations in Fig. 5, and 0 everywhere else. The method described above is identical to how the probing locations are set up using standard downsampling. The second way in which the probe locations are initialized uses cellular location knowledge that has already been acquired from previous slices in the 3-D sequence. For example, Fig. 3, shows that cell locations in adjacent slices are very similar. When stepping through the sampling process, it is efficient to rule out areas unlikely to contain any pertinent information. Fig. 6 shows an illustration of how to initialize the probe locations if we know approximately where the cell is located. We will elaborate on this in what follows. The initialization of these probe locations is identical to the method (a) with one added step—the application of a mask from the previous slice as shown here (the computation of the mask is given later in this section). Thus, the probing image for method (b), $p^{(b)}_{m,n,o}$ is given by

$$p^{(b)}_{m,n,o} = p^{(a)}_{m,n,o} \cdot \text{mask}_{m,n,o-1}.$$

We can, thus, express the probing image as

$$p_{m,n,o} = \begin{cases} p^{(a)}_{m,n,o}, & \text{method}(a) \\ p^{(b)}_{m,n,o}, & \text{method}(b). \end{cases}$$

These two methods for initializing the probe locations are used in two different situations: The first method is used when there is no information available about the location of the cell, while the second one is used when such information is available (for example, when slices at either previous time instants or previous locations along the third spatial dimension have already been acquired). To add more robustness to the system, the first method can also be used periodically even when knowledge about the location is available. Probing occurs until there are no more locations left to be examined.

After a location is probed and an intensity value is returned, it is compared to a threshold. The threshold is set by the user and determines the sensitivity of the algorithm. A lower threshold will raise the sensitivity and take more samples while a higher threshold will consider more locations to be uninteresting.

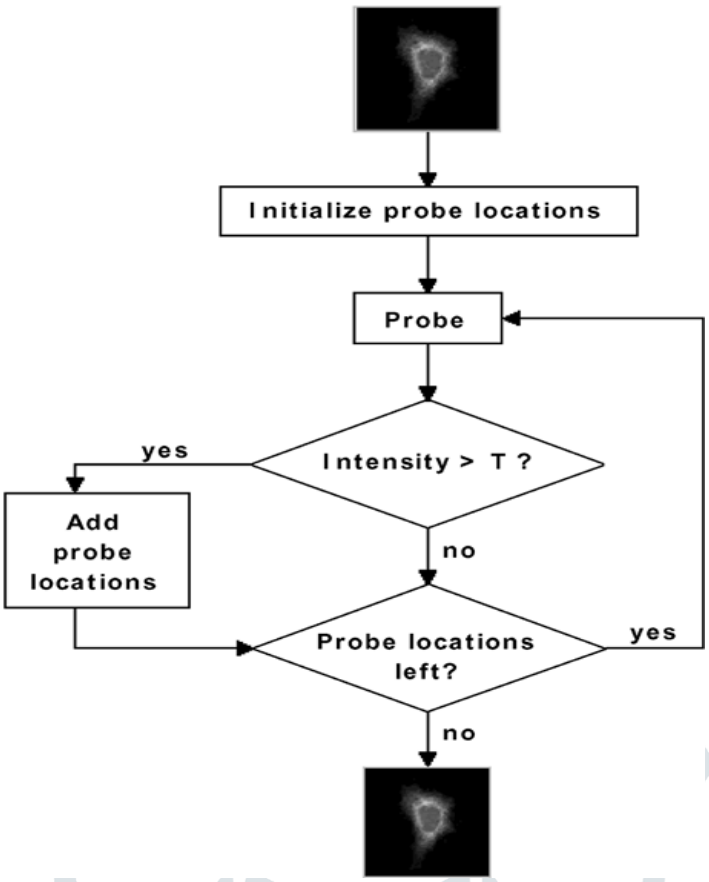

Fig. 4. Block diagram for the MR sampling algorithm

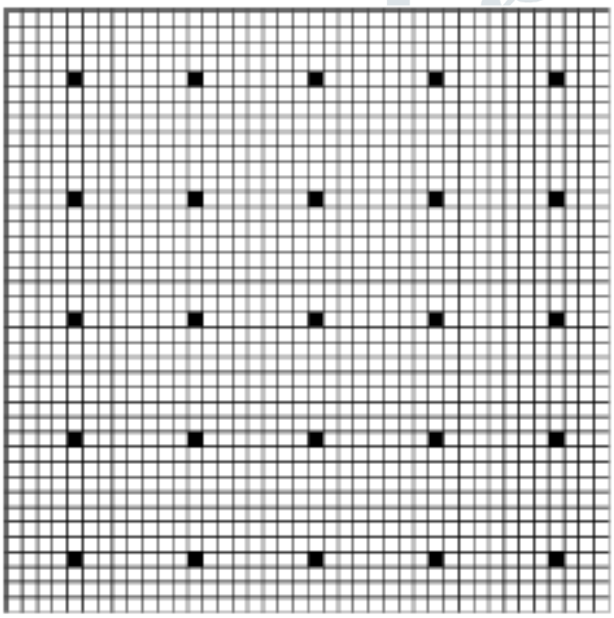

Fig. 5. Initial sampling grid for both the method (a), and the standard downsampling algorithm. Each block represents a possible probe location while the black blocks represent where a probe location has been initialized.

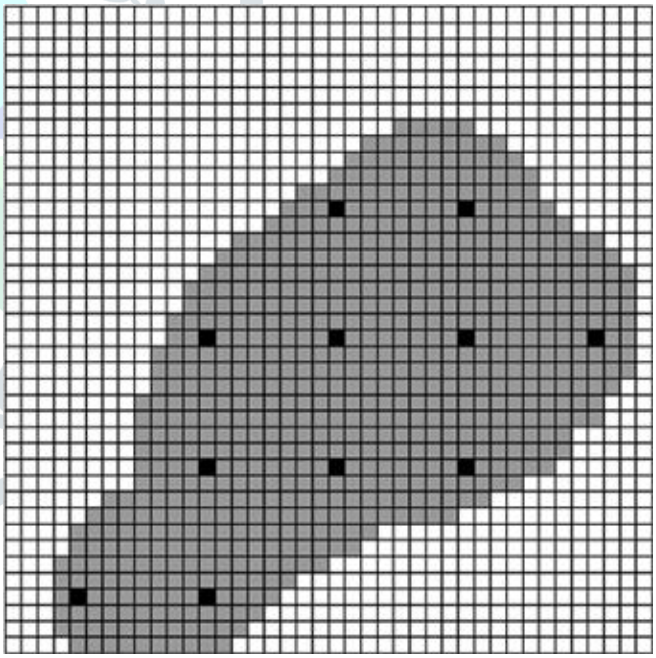

Fig. 6. Initial sampling grid for method (b). Each block represents a possible probe location. Black blocks represent where a probe location has been initialized. Gray blocks represent the locations where we assume important information is located. The probe locations are only set up in the area where the cell is believed to be located.

When a pixel's intensity is examined, one of two things occurs: If the value is greater than the threshold, then the value is stored in what is called a *foreground image*, $\boldsymbol{f}$. The foreground image contains all of the intensity values gathered from probes where the intensity exceeds the threshold

$$f_{m,n,o} = \begin{cases} x_{m,n,o}, & x_{m,n,o} > T \& (m,n) \in I \\ 0, & \text{otherwise.} \end{cases}$$

With this image, we associate the binary image ***fb*** where 1 signifies where the foreground image has positive intensities and 0 signifies no intensity

$$fb_{m,n,o} \begin{cases} 1, & f_{m,n,o} > 0 \\ 0, & \text{otherwise.} \end{cases}$$

After the current value exceeding the threshold is stored, new probes are added as shown in Fig. 7. The examined pixel can be thought to have a depth, *d*. The extended neighborhood is $c2^{l-d}$ from the current location. For our experiments, $c = 1.5.$ In the figure, the distance between probe locations (black pixels) is $2^l = 8, d = 0.$ In part (a), the gray pixels $(l = 3, d = 1)$ represent the probe locations added when the circled probe location reveals a value that is greater than or equal to the threshold. This is a recursive process and its next step is shown in part (b) of the same figure. This operation can also be thought of as the following convolution:

$$p^{(\text{new})}_{m,n,o} = fb * t$$

where $t_{m,n} \in \mathbb{R}^{(c2^{l-d}+1)\times(c2^{l-d}+1)}$ and

$$t_{m,n} = \begin{cases} 1, & m = 2^{l-d-1}k_m, \quad k_m = 0,\ldots,2c \\ & n = 2^{l-d-1}k_n, \quad k_n = 0,\ldots,2c \\ 0, & \text{otherwise.} \end{cases}$$

For example, with $l = 3$ and $c = 1.5,$ we have $t_{m,n} \in \mathbb{R}^{13\times13}$ and it equals 1 only for m, n= 0,4,8,12.
This process iterates until all of the probe locations identified by are probed. The index set *I* is also updated at this time

$$I^{(\text{new})} = \left\{(m,n)\ p^{(\text{new})}_{m,n,o} = 1\right\}$$

We then set $p = p^{(\text{new})}$ and $I = I^{(\text{new})}$ in preparation for a new iteration.

Each time a value is returned from a probe it is stored in what is called the background image *b*. This occurs regardless of whether or not the value exceeded the threshold. The background image consists of all the probed locations which have then been interpolated to the dimensions of the original image. When a location is probed, the value is placed in a temporary image *z* of the same dimensions as the original and initialized to all zeros. The probed value is then replicated to fill its proximity. The proximity is a subset of *z* that surrounds the probe location in the neighborhood of 2^{l-d} where *d* is once again the depth of the particular index value in *I*. All the locations in this subset take on the value of the probed location

$$z_{m+k_m,n+k_n,o} = \begin{cases} x_{m,n,o}, & k_m = -2^{l-d-1},\ldots,2^{l-d-1}-1 \\ & k_n = -2^{l-d-1},\ldots,2^{l-d-1}-1 \\ & (m,n) \in I. \end{cases}$$

Once all probing is completed, we can now construct the background image *b*, given by

$$b_{m,n,o} = (z * lp)_{m,n,o}$$

where *lp* is a lowpass filter. In our experiments, we used a simple averaging filter $lp \in \mathbb{R}^{8\times8}$ where $lp = 1/64$ everywhere.

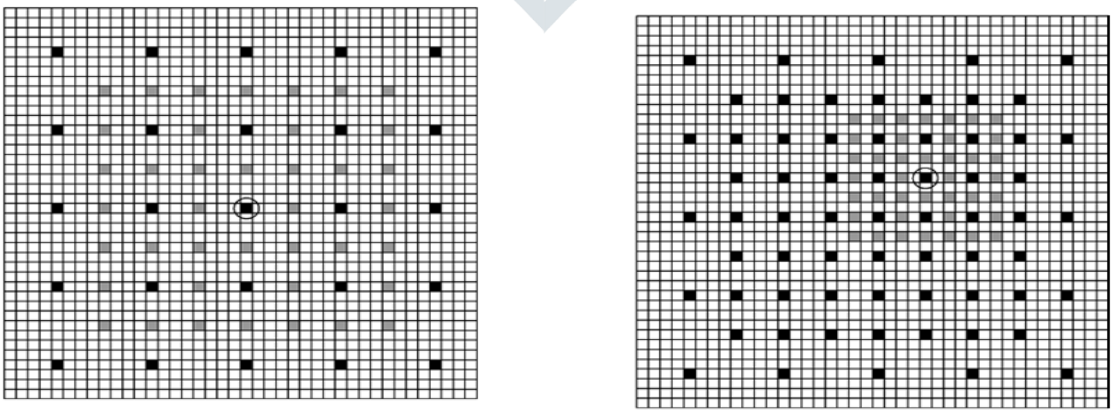

(a) (b)

Fig. 7. (a) Grid obtained when the circled probe location returns a value greater than the threshold. When this happens, the probe locations in gray are added. (b) When one of the gray locations from (a) returns an intensity greater than the threshold, the process continues recursively.

Now, we can construct the approximated image equal to the background image where the foreground image is without an intensity value

$$y_{m,n,o} = \begin{cases} f_{m,n,o}, & f_{m,n,o} > 0 \\ b_{m,n,o}, & \text{otherwise.} \end{cases}$$

To create a more efficient algorithm and save even more probes, we can use the information about the cell location from the previous slice that has been approximated. This is done by creating a mask. The mask examines the foreground image of the neighboring/previous slice.

This image is expanded by the morphological operation of dilation to create a mask that is larger than the area where the structure was located in the neighboring slice

$$\text{mask}_{m,n,o} = \begin{cases} 1, & (fb * s)_{m,n,o} > 0 \\ 0, & \text{otherwise} \end{cases}$$

where $s_{m,n,o} \in \mathbb{R}^{2^l \times 2^l}, s_{m,n,o} = 1$ everywhere. This compensates for any growth, movement or displacement of the cell. In the subsequent slice, we will only initialize the probe locations that lie in the region where the mask is located. If we consider our board game example again, it becomes clear how the masking operation works. Let us modify the game so that multiple rounds of the game are allowed. In the subsequent rounds, the opponent's pieces are limited to how far they can travel from the prior round. With this restriction, an efficient search would begin in only those neighborhoods where the opponent's pieces were located in the earlier round. For 2-D cellular data sets, the masking step is omitted.With those data sets, the algorithm never assumes to have knowledge of the cell location and always initializes the probe locations using the first method of initialization described earlier in this section.

IV. COMPARATIVE STUDY

In the last several decades, numerous biomedical imaging techniques were developed, ranging from the whole organism level (millimeter resolution) down to the single molecule level (nanometer resolution) (Murphy, 2001; Tsien, 2003). Some of the most widely used biological imaging methods include confocal or two-photon laser scanning microscopy (LSM) (Pawley, 2006), scanning or transmission electron microscopy (EM) (Bozzola and Russell, 1999), etc. Novel imaging techniques such as PALM (Betzig et al., 2006), STORM (Rust et al., 2006), STED (Hell, 2003) that far surpass the resolution of conventional optical microscopes currently can pinpoint the location of individual proteins that are only several nanometers apart. Along with the dramatic advances of many related techniques such as image signal digitization and storage, biological tissue labeling [e.g. green fluorescent proteins (GFP) and enhanced
GFP (EGFP) (Heim et al., 1995; Shimomura et al., 1962), Dronpa (Ando et al., 2004), Brainbow combinatorial labeling (Livet et al., 2007)], the number of biological images (e.g. cellular and molecular images, as well as medical images) acquired in digital forms is growing rapidly. Large bioimage databases such as Allen Brain Atlas (Lein et al., 2007) and the Cell Centered Database (CCDB; Martone et al., 2002) are becoming available. These image data could involve (1) two-dimensional (2D) or 3D spatial information, (2) multiple colors which may correspond to various molecular reporters, (3) 4D spatio-temporal information for developing tissues or moving cells,
(4) various co-localized biological signals such as mRNAexpression levels of different genes (Lein et al., 2007; Long et al., 2007b; Peng et al., 2007) or (5) other screening experiments related to RNAinterference (RNAi), chemical compounds, etc. (Echeverri and Perrimon, 2006; Moffat et al., 2006; Sepp et al., 2008). Analyzing these images is critical for biologists to seek answers to many biological problems, such as differentiating cancer cell phenotypes (Long et al., 2007a), categorization of neurons (Jefferis et al., 2007).

V. RESULTS AND DISCUSSION

a) Acquisition Time

A 2-D data field having dimensionality *m* x *n* has *mn* total probe locations. Our MR approach reduces the number of probed locations to $mn/2^{2l} + s$, where *s* is an approximate number of probe locations that exceed the threshold *T*. Since $mn/2^{2l} + s \leq mn$, the amount of compression depends on (determined by *T*), and the data set being acquired.

Typically, $s \gg mn/2^{2l}$ indicating that the majority of probes in the MR algorithm are spent acquiring data that exceeds the threshold, in which case, the number of probe locations depends more on the number of samples exceeding the threshold and less on the dimensions of the acquisition field. The number of probes for MR will be between (when all samples exceed threshold) and $mn/2^{2l-1}$ (when *s* approaches $mn/2^{2l}$). Each pixel probed in a data set requires an excitation time for the fluorescence to be detected by the microscope. The excitation time cost is proportional to the percentage of samples kept, that is, to $1/2^{2l} + s/(mn)$.

Excitation time will be faster for the data set proportional to the number of samples kept, a factor of $1/2^{2l} + s/(mn)$. The time associated with adding additional probes is of $O(1)$, a negligible amount. The increased acquisition time cost depends solely on the confocal scanning microscope's ability to change laser spot.

b). Data Storage

The data storage requirement of this system is similar to that of the normal, line-by-line, pixel-by-pixel acquisition. The output of the MR system is a data set that matches the dimensions of the total cellular field being captured. This approximated data set has the same dimensionality as the original data set. Since the MR algorithm approximates the original data set, there is no further saving in terms of storage.

c). Distortion of Input

The distortion of input is an important topic and is discussed in greater detail in Section V.We compare our simulated acquisition to the simulations of nonadaptive approaches and observe the distortion in both a mean-squared error (MSE) and classification sense.

d). Robustness to Noisy Input

The MR acquisition is not impervious to noise. If the cellular field being imaged is noisy, then the MR algorithm will use additional samples to capture noisy areas. The amount of noise captured will depend on the noise distribution, intensity of noise and the threshold of acquisition. Thus, the algorithm will adapt itself to a noisy input, probing more samples and resulting in lower overall compression.

e). Implementation

Confocal scanning microscopes have the precision to capture any pixel in the cellular field. The cost of implementing this system is the reprogramming of the microscope to follow a different protocol as explained in Section III, as well as the time needed to move from pixel to pixel. These issues will be addressed in detail during the implementation stage of this project.

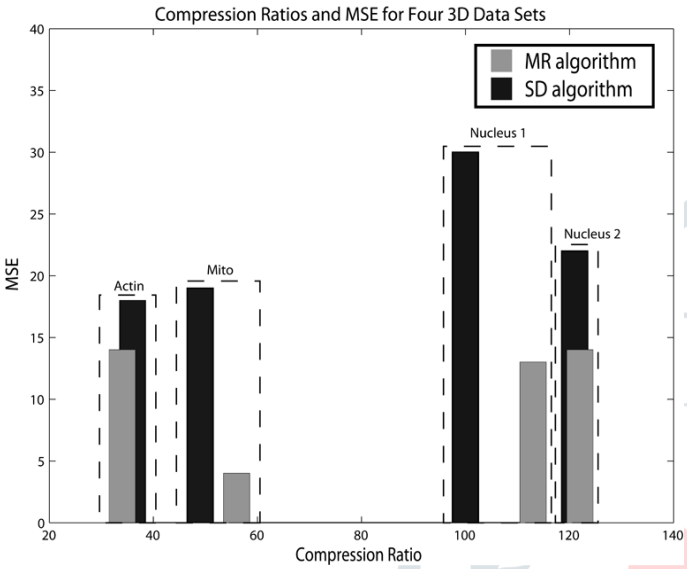

Fig. 8. Compression ratios and MSE for four 3-D data sets. The results are given for the MR algorithm and the standard algorithm.

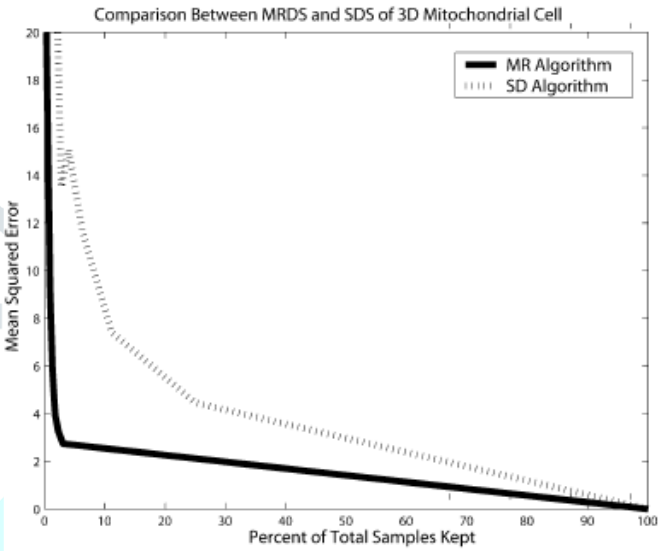

Fig.9. Rate-distortion curves for MR downsampling compared to standard downsampling with bilinear interpolation.

V. APPLICATIONS

Just like many other engineering fields, bioimaging is application-driven, as one can see from the following non-exclusive instances.

a) high-content analysis of cellular phenotypes

Large-scale screening of cellular phenotypes, at whole-cell or sub-cellular levels, is of importance for determination of gene functions, delineating cellular pathways, drug discovery and even cancer diagnosis. The CellProfiler system was developed to screen cellular images rapidly and gather information such as number of cells, size and other morphological features of cells, per-cell protein levels, cell cycle distribution, etc.

b) Atlas building for model organisms

Single-cell analysis for an entire animal is useful for understanding the cell functions, such as the neuronal circuit mapping based on 3D cellular images of a brain. This task is possible if the cells have unique identities, indicated by the stereotypy of their 3D locations, 3D morphology, birth orders (lineages), gene expression patterns or other functional properties. Several systems do have these distinct properties.

c) Understanding the dynamic processes in cells and living organisms

For intracellular processes, the microtubule, one class of the cytoskeleton polymers that is constantly assembled and disassembled, receives much attention in studies of various cell functions, e.g. cell division. By imaging GFP fused to the distal ends of microtubules, it is possible to analyze the different dynamic patterns of microtubules, such as the velocity and acceleration, for mutants or under other conditions. Computationally, the microtubule growing, shortening and other dynamic patterns can be tracked in time-lapse microscopy images, via mixture analysis of hidden Markov models.

VI. FUTURE SCOPE

Automated tracking and analysis of moving objects in image sequences has been and continues to be one of the major themes in digital image analysis research. This is not surprising in view of its many applications in video surveillance, multimedia services, automated vehicle guidance and driver assistance, remote sensing and meteorology, and medical imaging. It is also a recurring theme in molecular biology. By their very nature, biomolecular systems are dynamic, and it is one of the major challenges of biomedical research and pharmaceutical industries in the postgenomic era to unravel the spatial and temporal relationships of these complex systems and to devise strategies to manipulate them. Results in this area can be expected to have profound social and

economic impact in the near future, as they can be harnessed to improve human health and well-being. Studies into biomolecular dynamics generate ever increasing amounts of image data. To be able to handle these data and to fully exploit them for describing biological processes on a quantitative level and building accurate mathematical models of dynamic structures, computerized motion analysis is rapidly becoming a requisite.

CONCLUSION

We presented a scheme for adaptive MR acquisition of fluorescence microscopy data sets in the context of classification of proteins based on their subcellular locations. We found that the MR down sampling outperforms standard down sampling due to an intelligent acquisition scheme. In a rate-distortion sense, our algorithm outperforms the standard one because it retains the high frequencies and saves samples where low frequencies are present. In terms of classification accuracy, our algorithm shows great promise as it significantly reduces the number of samples acquired while minimally affecting the classification accuracy. Future work includes implementing our algorithm as the microscope's scanning protocol.

REFERENCES

[1] "The Colored Revolution of Bioimaging" IEEE SIGNAL PROCESSING MAGAZINE [20] MAY 2006 1053-5888/06/$20.00©2006IEEE

[2] M. Velliste and R. F. Murphy, "Automated determination of protein subcellular locations from 3-D fluorescence microscope images," in Proc. IEEE Int. Symp. Biomedical Imaging, Washington, DC, 2002, pp. 867–870.

[3] IEEE TRANSACTIONS ON IMAGE PROCESSING, VOL. 14, NO. 9, SEPTEMBER 2005 "An Adaptive Multirate Algorithm for Acquisition of Fluorescence Microscopy Data Sets" Thomas E. Merryman, and Jelena Kova˘cevic.

[4] "Bioimage informatics: a new area of engineering biology" Hanchuan Peng Janelia, Advance Access publication July 4, 2008, pages 1827–1836

[5] "TRACKING NON-RIGID STRUCTURES IN COMPUTER SIMULATIONS" Abel Gezahegne and Chandrika Kamath IEEE International Conference on Image Processing San Diego, CA, United States October 12, 2008.

[6] ISBI'08, IEEE International symposium on bioimaging, April 2008. "BREAST CANCER DETECTION BY TIME REVERSAL IMAGING" Yuanwei Jin, Jos´e M.F. Moura, and Yi Jiang, Mellon University Pittsburgh, PA 15213.

[7] "Tracking in Molecular Bioimaging" Erik Meijering Ihor Smal Gaudenz Danuser21Biomedical Imaging Group Rotterdam, Erasmus MC—Universitym, The Netherlands, vol. 23, no. 3, May 2006, pp. 46–53.